Electronic structure and photoabsorption of Ti3+ ions in reduced anatase and rutile TiO2

Journal:	*Physical Chemistry Chemical Physics*
Manuscript ID	CP-ART-04-2018-002648.R1
Article Type:	Paper
Date Submitted by the Author:	25-May-2018

Complete List of Authors:	Wen, Bo; Beijing Computational Science Research Center, Hao, Qunqing; Dalian Institute of Chemical Physics Yin, Wen-Jin; Beijing Computational Science Research Center, Zhang, Le; Research Center for Eco-Environmental Sciences, Chinese Academy of Sciences, Wang, Zhiqiang; Xidian University, School of Physics and Optoelectronic Engineering Wang, Tianjun; State Key Laboratory of Molecular Reaction Dynamics, Dalian Institute of Chemical Physics, Chinese Academy of Science Zhou, Chuanyao; Dalian Institute of Chemical Physics, State Key Laboratory of Molecular Reaction Dynamics Selloni, Annabella; Princeton University, Chemistry Yang, Xueming; Dalian Institute of Chemical Physics , Liu, Li-Min; Beijing Computational Science Research Center,

Journal Name

ARTICLE

Electronic structure and photoabsorption of Ti^{3+} ions in reduced anatase and rutile TiO_2†

Received 00th January 20xx,
Accepted 00th January 20xx

DOI: 10.1039/x0xx00000x

www.rsc.org/

Bo Wen‡[a], Qunqing Hao‡[b, e], Wen-Jin Yin[a], Le Zhang[a], Zhiqiang Wang[b, f], Tianjun Wang[b], Chuanyao Zhou*[b], Annabella Selloni[c], Xueming Yang[b], Li-Min Liu*[d, a]

We have used two-photon photoemission (2PPE) spectroscopy and first-principles density functional theory calculations to investigate the electronic structure and photoabsorption of the reduced anatase TiO_2 (101) and rutile TiO_2 (110) surfaces. 2PPE measurements on anatase (101) show an excited resonance induced by reduced Ti^{3+} species centered around 2.5 eV above the Fermi level (E_F). While this state is similar to that observed on the rutile (110) surface, the intensity of the 2PPE peak is much weaker. Calculation of the oscillator strengths of the transitions from the occupied gap states to the empty states in the conduction band show peaks between 2.0-3.0 eV above the conduction band minimum (CBM) on both surfaces, confirming the presence of empty Ti^{3+} resonances at these energies. Although the crystal field environment of Ti ions is octahedral in both rutile and anatase, Ti^{3+} ions exhibit distinct *d* orbital splittings, due to different distortions of the TiO_6 units. This affects the directions of the transition dipoles from the gap states to the conduction band, explaining the polarization dependence of the 2PPE signal in the two materials. Our results also show that the Ti^{3+} induced states in the band gap are shallower in anatase than in rutile. Most importantly, *d*→*d* transitions from the occupied gap states to the empty Ti^{3+} excited states in anatase can occur at energies well below 3 eV, consistent with the observed visible-light photocatalytic activity of Ti^{3+} self-doped anatase.

Introduction

TiO_2 is an attractive photocatalyst for many applications[1-9], but its performance is limited by the large band gap, requiring the use of ultraviolet light for photoexcitation[3, 10]. As efforts at increasing TiO_2's visible light activity by narrowing its band gap through doping have proven difficult[11-14], recently attention has been directed to the potentially beneficial role of reduced Ti^{3+} ions. However, while there is evidence that the photoactivity of TiO_2 in the visible could be substantially enhanced by high concentrations of Ti^{3+} ions[15-21], understanding of the mechanism of this enhancement is still limited.

Ti^{3+} ions in TiO_2 are usually associated with oxygen vacancies (O_vs), whose excess electrons tend to localize in the 3d orbitals of nearby Ti atoms forming states with energies in the band gap. Many properties of the gap states have been studied extensively, including their energetics, localization and transport behaviour, but less is known about their photoexcitation, which is crucial for understanding their role in TiO_2's photoactivity. Experimental studies have generally been performed by two-photon photoemission spectroscopy (2PPE), an optimal technique for the study of excited states. Using 2PPE, Onda *et al.* first identified a resonant state at about 2.3 eV above the conduction band minimum (CBM), which they originally ascribed to a wet electron state induced by water adsorption.[22, 23] Thornton *et al*. observed a similar feature at 2.7 eV[24], and suggested that this peak originates from *d-p* transitions from the gap state to states induced by surface hydroxyls. Argondizzo *et al*. also observed a resonant transition from Ti 3*d* defect states, and attributed it to transitions between Ti 3*d* bands of t_{2g} and e_g symmetry.[25] A more precise assignment was proposed by Wang *et al*., who showed that both the gap state and the resonant state above the CBM originate from the Ti^{3+} ions, and $3d \rightarrow 3d$ transitions from the gap states to the empty resonant states affect the photoabsorption significantly.[19]

While providing useful information, a limitation of all the above studies is that they were performed on a single well-defined surface, the rutile TiO_2 (110) surface, a typical model system for surface science studies of TiO_2. On the other hand, only a preliminary report is available for anatase (101)[26], the majority surface of the TiO_2 form that is generally used in photocatalysis and other energy conversion applications. A distinctive feature of anatase (101) with respect to rutile (110) is its lack of surface O_vs, since

[a] *Beijing Computational Science Research Center, Beijing, 100193, P. R. China. Email: limin.liu@csrc.ac.cn*
[b] *State Key Laboratory of Molecular Reaction Dynamics, Dalian Institute of Chemical Physics, Chinese Academy of Science, 457 Zhongshan Road, Dalian, 116023, Liaoning, P. R. China. Email: chuanyaozhou@dicp.ac.cn*
[c] *Department of Chemistry, Princeton University, Princeton, New Jersey 08544, United States.*
[d] *School of Physics and Nuclear Energy Engineering, Beihang University, Beijing 100191, P. R. China. Email: liminliu@buaa.edu.cn*
[e] *Science and Technology on Surface Physics and Chemistry Laboratory, P.O. Box No. 9-35, Huafengxincun, Jiangyou City, Sichuan Province, 621908, P. R. China.*
[f] *School of Physics and Optoelectronic Engineering, Xidian University, Xi'an, 710071, P. R. China.*
† Electronic Supplementary Information (ESI) available: methods and experimental analysis on photon polarization, as well as additional data and figures.
‡ Who made equal contribution to this work.
* Corresponding authors.

these defects prefer to reside in subsurface and deeper layers than at the very surface of anatase.[27, 28] Also at variance with rutile, there is evidence of both deep (strongly localized) and shallow (more extended) Ti^{3+}-like gap states in anatase[29-34]. Therefore, understanding the excited state properties of reduced anatase is of considerable scientific interest, as well as important for applications.

The aim of this work is to provide a detailed characterization of the excited state properties of the reduced (101) surface of anatase (*A*-TiO_2), the technologically most relevant form of TiO_2. Using 2PPE measurements in combination with density functional theory (DFT) calculations, we show that Ti^{3+} species in *A*-TiO_2 have both similar and distinct features in comparison to rutile (*R*-TiO_2). Most importantly, transitions from the gap states to the corresponding Ti^{3+} resonant states can induce visible light absorption and thus enable photoactivity in this spectral region.

Method

Experimental details

2PPE experiments were carried out in an ultrahigh vacuum (UHV) apparatus with a base pressure better than 5×10^{-11} mbar.[35] The *A*-TiO_2(101) sample (Princeton Scientific Corp.) was prepared by cycles of Ar^+ sputtering and UHV annealing at 850 K until the impurity concentration was below the detection limit of X-ray photoelectron spectroscopy (XPS) and low energy electron diffraction (LEED) showed a clear sharp (1×1) pattern. The second harmonic (SH, 2.95 eV – 3.59 eV) of a Ti: Sapphire oscillator (MaiTai eHP DeepSee, Spectra-Physics) was delivered in pulses of 90-fs duration and 1.5-nJ at 80-MHz repetition rate for the two-photon excitation. The laser incident plane was at about 30 degrees relative to the [010] direction of the anatase (101) surface. One-photon photoemission measurements were performed using a helium lamp (UVS 10/35, SPECS) at the photon energy of 21.2 eV. Photoelectrons were collected with a hemispherical electron energy analyzer (PHOIBOS 100, SPECS) and the Fermi level was measured from a tantalum plate in direct contact with the sample. All photoemission measurements were performed with a TiO_2 sample temperature of 120 K. Since the band gap and the work function of the n-type *A*-TiO_2(101) sample were 3.2 and 4.8 eV respectively, two-photon excitation using SH photons could emit electrons exclusively from the band gap state.

Computational setup

Spin polarized density functional theory calculations were performed with the CP2K/Quickstep package,[36] which uses a hybrid Gaussian and plane-waves approach. Core electrons were described with norm-conserving Goedecker, Teter, and Hutter (GTH) pseudopotentials.[37] The wave functions of the valence electrons were expanded in Gaussian functions with molecularly optimized double-zeta polarized basis sets (m-DZVP).[38] For the auxiliary basis set of plane waves a 280 Ry cut-off was used. Reciprocal space sampling was restricted to the Γ point. The Heyd, Scuseria, Erzernhof (HSE06) functional[39-41] with a fraction α = 25% of Hartree-Fock (HF) exchange was typically employed. However, to check the accuracy[42] of the results, a few additional hybrid functionals have been used, notably: a modified PBE0[41, 43] functional with $\alpha = 1/\epsilon_\infty$, where ϵ_∞ is the static electronic dielectric constant of the material[44] (specifically α =17.5% and 15.8% for anatase and rutile, respectively, using experimentally determined ϵ_∞ values for the two polymorph[45, 46]; and the B3LYP[47, 48] functional, with α = 20%.

The *A*-TiO_2(101) surface was modeled using periodically repeated slabs of three and four TiO_2 tri-layers with a vacuum separation between slabs of about 15 Å. We used slabs of 3 tri-layers with (1×3) (10.21Å×11.33Å) and (1×4) (10.21Å×15.06Å) surface supercells for the hydroxylated and doped surface, respectively. We employed slabs of both 3 and 4 tri-layers for the reduced surface with a subsurface O-vacancy in order to check the convergence of the results with respect to the anatase thickness, see **Table S1** of Supporting Information (SI). The hydroxylated surface was modeled by adding one or more hydrogen atoms on the bridging oxygen sites; reduced surfaces were modeled by removing a subsurface oxygen atom. All atoms in the slab were relaxed until the maximum residual force was less than 0.02 eV/Å. Calculations for the *R*-TiO_2 (110) surface were performed using periodically repeated slabs of four TiO_2 tri-layers with a (4×2) (11.84 Å×12.99 Å) surface cell. We modeled hydroxylated *R*-TiO_2 (110) by adding one or more hydrogen atoms to the surface bridging oxygen sites, and reduced *R*-TiO_2 (110) by a removing a surface bridging oxygen atom to create a surface oxygen vacancy.

The oscillator strength in the $\vec{e}_\mu$ direction, f_{cv}^{μ}, was calculated from the expression:[49]

$$f_{cv}^{\mu} = \frac{2m_e(E_c-E_v)}{\hbar^2}\left|\langle v|\vec{e}_\mu\cdot\vec{r}|c\rangle\right|^2 \quad (1)$$

Using the relationship between position and momentum operators $(r_\mu)_{vc} = \frac{i\hbar}{m_e(E_c-E_v)}(p_\mu)_{vc}$, equation (1) can be transformed to:

$$f_{cv}^{\mu} = \frac{2}{m_e(E_c-E_v)}\left|\langle v|p_\mu|c\rangle\right|^2 \quad (2)$$

where $\langle v|$ denotes a Kohn-Sham orbital corresponding to a state in the valence band (VB) or an occupied gap state and $|c\rangle$ denotes a Kohn-Sham orbital corresponding to an unoccupied MO above E_F. E_c and E_v denote the eigenvalues corresponding to $|c\rangle$ and $\langle v|$, respectively. p_μ is the momentum along the $\vec{e}_\mu$ direction. The oscillator strength was also utilized to evaluate the imaginary part of the dielectric function as [50, 51]:

$$\epsilon_2^{\mu}(\omega) = \frac{2\pi^2e^2\hbar}{m_e\omega}\sum_{vc} f_{vc}^{\mu}\,\delta(\omega_{cv}-\omega) \quad (3)$$

where v and c denote valence and conduction band states. In our calculations, the sum over the valence band states was restricted to the gap state.

Results and discussion

Experimental results

Previous 2PPE studies on R-TiO_2(110) by our group were performed on an hydroxylated surface[19], which is more relevant to real photocatalysis compared to the clean surface. Unlike R-TiO_2(110), however, A-TiO_2(101) does not exhibit surface oxygen vacancies,[52] making it difficult to create hydroxyls through dissociation of water at such sites. We tried to introduce surface hydroxyls using various methods including methanol photo dissociation,[53, 54] photolysis of trimethyl acetic acids[55] and atomic hydrogen dosing[56], as used on R-TiO_2(110). Unfortunately, besides producing surface hydroxyls, these methods inevitably introduce other species such as water (from hydration of methanol, trimethyl acetic acids and heating of the

cracking zone) onto the surface. Even worse, we could not control the amount of water, which is known to significantly affect the intensity of 2PPE spectra on R-TiO_2(110).[23, 57] In fact, 2PPE spectra on A-TiO_2(101) are also water coverage sensitive. In order to remove water and other reaction species, one needs to heat the substrate to temperatures above 300 K, which results in the diffusion of H atoms into the bulk of A-TiO_2(101), as suggested by our UPS measurements and also by calculations.[58] We found that it is essentially impossible to assess the amount of surface hydroxyls during the 2PPE measurements using current experimental techniques. As a result, all the photoemission spectra in this work were acquired from the clean reduced A-TiO_2(101) surface.

Figure 1a shows the polarization dependent 2PPE spectra on a clean *A*-TiO_2(101) at a photon energy of 2.95 eV. These spectra are quite similar to those for *R*-TiO_2(110) with the incident plane along the [1$\bar{1}$0] direction (see representative spectra in **Figure 1b**).[19] An additional feature *F* is detected in *p*-polarized 2PPE (*p*-2PPE) when

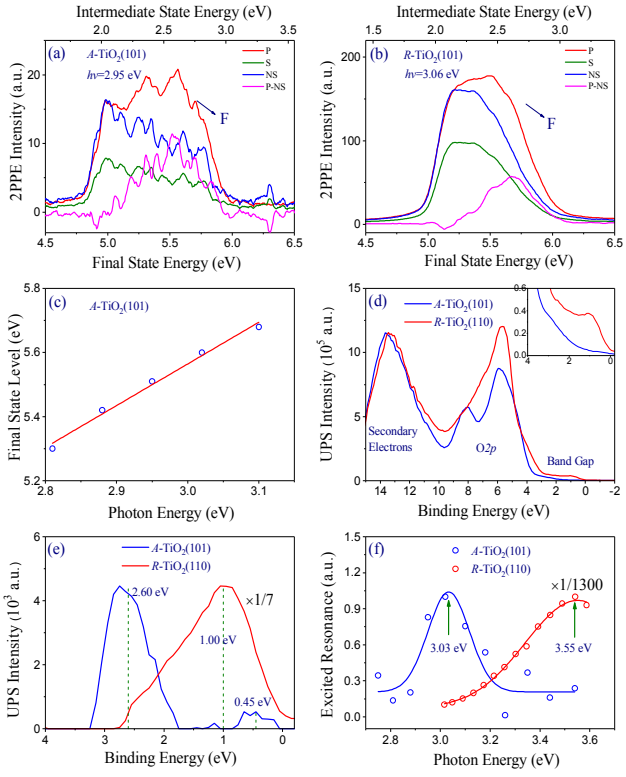

Figure 1 (a) Typical 2PPE spectra for the clean *A*-TiO_2(101) surface acquired with a photon energy of 2.95 eV. The spectra were measured with both *p*-polarized (P) and *s*-polarized (S) light. For comparison, S was normalized to P at the secondary electron signal edge. P-NS denotes the difference spectra, which was obtained by subtracting the normalized *s*-polarized data (NS) from the *p*-polarized data. The signal was integrated from -5 degree to +5 degree. Energies are measured with respect to E_F; those in the top X-axis refer to the intermediate state, before absorption of the second photon. (b) 2PPE spectra for the clean *R*-TiO_2(110) surface acquired with a photon energy of 3.06 eV. Please note the different scale in (a) and (b). (c) Photon energy dependence of the final state level in 2PPE. The slope is close to unity, suggesting the resonance signal comes from an intermediate state, i.e., excited state. (d) Valence electronic structure of *A*-TiO_2(101) and *R*-TiO_2(110) measured with identical experimental parameters. The inset graph emphasizes the band gap states on both TiO_2 surfaces. (e) Detailed electronic structure in the band gap obtained by subtracting the Tougaard background of the UPS spectra in Figure 1d. Note the signal from *R*-TiO_2(110) has been divided by 7. (f) Photon energy dependence of the normalized excited resonance in 2PPE on both *A*-TiO_2(101) (blue circle) and *R*-TiO_2(110) (red circle). On each surface, the photon energy dependent 2PPE spectra were normalized at the secondary electron edge and the excited resonance in *p*-2PPE was then integrated. The data points were fitted by a Gaussian function.

compared to *s*-polarized 2PPE (*s*-2PPE); the difference between *p*-2PPE and the normalized *s*-2PPE at the secondary electron edge, is a 0.48 eV wide peak centred at 5.50 eV; linear fitting of the photon energy dependence (**Figure 1c**) of the final state level yields a slope close to one, suggesting the additional feature *F* comes from an intermediated state; since no adsorbates are present on the *A*-TiO_2(101) surface, we can conclude there is an intrinsic excited state located at 2.55 eV above the Fermi level on this surface. No angular distribution of the excited resonance was detected, suggesting it is a rather localized state. Time-resolved measurements showed the two-pulse correlation from the excited state to be identical to the autocorrelation of the 2PPE pulses, implying that the lifetime of the excited state is much shorter than the pulse width (90 fs).

An important difference between the 2PPE signals from the clean *A*-TiO_2(101) and *R*-TiO_2(110) surfaces is the intensity. Although the photon energy chosen for the 2PPE acquisition on both TiO_2 surfaces are within 3±0.06 eV, the 2PPE intensity on *R*-TiO_2(110) (**Figure 1b**) is about 8 times larger than that on *A*-TiO_2(101) (**Figure 1a**). To find out the reason of the significant 2PPE intensity difference on these two surfaces, we studied the band gap states, which are the initial states in the 2PPE measurements, by ultraviolet photoelectron spectroscopy (UPS) using the He□line. **Figure 1d** compares the valence electronic structure of *A*-TiO_2(101) and *R*-TiO_2(110) measured by UPS with identical experimental setups. The UPS spectra can be divided into three regions: the secondary electron signal, centered at a binding energy of 13.4 eV, the O 2*p* signal of the TiO_2 surface, between 10 and 3 eV, and the band gap states signal, below 3 eV. The valence band maximum (VBM) of *A*-TiO_2(101) is at lower energy (higher binding energy) compared to the VBM of *R*-TiO_2(110), which is consistent with the band gap difference between anatase and rutile.[59] The band gap states also show significant differences (see inset graph of **Figure 1d**): in contrast to the high DOS with a binding energy of 1 eV on *R*-TiO_2(110), *A*-TiO_2(101) has an extremely weak signal in the band gap, in agreement with previous reports indicating that there are essentially no oxygen vacancies on this surface.[52] Further analysis of the band gap states by subtracting the Tougaard background of the UPS spectra in **Figure 1d** yields the detailed structure in the band gap (**Figure 1e**). The band gap structure of *R*-TiO_2(110) shows a broad peak with a maximum around 1.0 eV, which is characteristic of the polaronic defect-induced states on this surface.[60] Different from *R*-TiO_2(110), the band gap structure of *A*-TiO_2(101) consists of two separate features, a peak at about 2.60 eV and a smaller feature at about 0.45 eV. The energy level together with the intensity of the signal around 2.60 eV correlates with the excitation of the O 2*p* states by the satellite lines of He I. From the energy difference point of view, the signal around 0.45 eV is not interfered by the satellite lines. Therefore, it is likely to represent the band gap state of *A*-TiO_2(101).

To confirm this result, we tuned the 2PPE photon energy so as to find the resonance of the transitions between the gap states and the excited states on the *A*-TiO_2(101) surface (**Figure 1f**). By combining the energy of the resonance with the measured energy level of the excited states, we can then infer the energies of the initial states.[61] On *R*-TiO_2(110), the resonant photon energy in 2PPE is at 3.55 eV,[19] a value reproduced in the present study (red circles in **Figure 1f**). On *A*-TiO_2(101), although the energy level of the excited states is

similar to that on *R*-TiO_2(110), the resonant photon energy in 2PPE is 0.52 eV lower, suggesting that the center of the initial states is 0.48 eV below the Fermi level, in agreement with the level position obtained by UPS. The weak signal at 0.45 eV in the UPS spectra may be thus ascribed to the gap states of *A*-TiO_2(101). Such shallow gap states in anatase have been reported previously.[31, 62] The peak intensity of the band gap states on *R*-TiO_2(110) is about 65 times that on *A*-TiO_2(101), largely explaining the difference in the 2PPE intensities of the two materials.

Theoretical results

We further investigate the electronic structure of reduced *A*-TiO_2(101) with subsurface oxygen vacancies by means of hybrid density functional calculations, and compare the results to analogous calculations for *R*-TiO_2(110) with surface O_vs. **Figure 2** shows the projected DOS of Ti^{4+} (a), and Ti^{3+} (b, c) ions in pristine and reduced *A*-TiO_2(101) slabs, computed using HSE06 (a, b), which is widely used for oxide materials, and the $1/\epsilon_\infty$ PBE0 functional (c). In pristine *A*-TiO_2(101), the octahedral field splits the *d* states of Ti^{4+} ions into t_{2g} and e_g orbitals (**Figure 2a**)[63]. In reduced *A*-TiO_2(101), the nominal t_{2g}^1 configuration of Ti^{3+} ions undergoes a Jahn-Teller splitting.[60, 64] The occupied *d* orbital, with predominant d_{xz}/d_{yz} character, is stabilized and splits from the other *d* orbitals of the t_{2g} manifold to form a state in the band gap around 1 eV below the CBM. At the same time, the remaining unoccupied t_{2g} orbitals upshift in energy, and give rise to resonant states in the range 2.0-3.0 eV above the CBM (highlighted by the pink shading in **Figure 2b, c**).

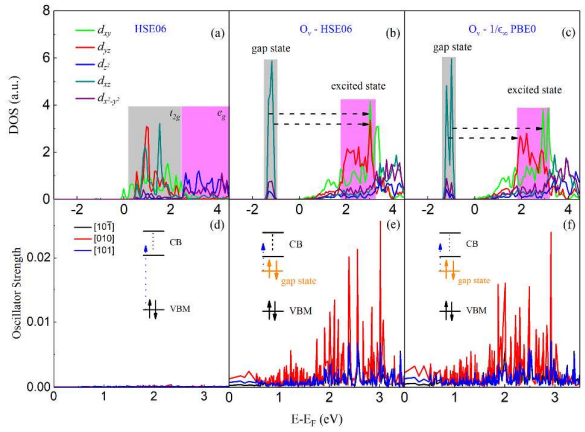

Figure 2 Projected DOS (upper panels) and oscillator strengths (lower panels) of: (a, d) Ti^{4+} ions in pristine anatase (101), calculated with HSE06; (b, e) and (c, f) Ti^{3+} ions in anatase (101) with one subsurface O-vacancy, calculated with HSE06 and $1/\epsilon_\infty$ PBE0 (α = 17.5%), respectively. In (a), the grey and pink regions correspond to t_{2g} and e_g states, respectively. In (b, c), the grey and pink regions represent the occupied gap state and empty resonant state, respectively. In (d), the oscillator strengths refer to transitions from the VBM state to the CB (indicated by blue dashed arrow). In (e, f) the oscillator strengths refer to transitions from the gap state to the CB. The black, red and blue lines indicate the components along [10$\bar{1}$], [010] and [101] directions, respectively. Simplified MOs or transitions near the band gap are illustrated in each panel.

Evidence for the *d* orbital character of the gap and resonant states of Ti^{3+} ions is presented in **Figure S1** (SI), while computed band gap energies and positions of the defect states relative to the CBM are reported in **Table S1** (SI). As shown in this Table, hybrid functionals typically overestimate the anatase band gap (as inferred from the difference between the CBM and VBM Kohn-Sham energies). At the same time, the predicted defect state energy levels are much deeper than the state at about 0.45 eV below E_F detected in our experiment.[65, 66] This difference may be related to different locations of the O_vs in our calculations and in experiment. It was indeed shown that near-surface O_vs (as considered in our calculations) induce deeper energy levels in the band gap than bulk O_vs.[30] It is therefore likely that the signal at 0.45 eV observed in our experiment originate for O_vs farther below the surface than those examined in our DFT calculations.

Oscillator strengths express the probability of absorption of electromagnetic radiation in transitions between occupied and unoccupied orbitals. To highlight the effect of Ti^{3+} ions on the absorption, we computed the oscillator strengths on pristine and reduced *A*-TiO_2(101), considering transitions from the VBM (**Figure 2d**) or from the gap states (**Figure 2e, f**) to the CB. The oscillator strengths of the VBM→CB transitions on pristine anatase (**Figure 2d**) are all very small in the energy range 0~3.5 eV above the CBM (similar results are obtained also for the VBM-1→CB and VBM-2→CB transitions). In contrast, the oscillator strengths of the transitions from the gap states to the CB show several sharp peaks on the reduced surface, especially in the range 2.0-3.0 eV. This feature appears not only in the HSE06 results but also in the oscillator strengths calculated with $1/\epsilon_\infty$ PBE0 (**Figure 2c, f**), and B3LYP (**Figure S2** in SI). Since the PDOS of Ti^{3+} ions on these surfaces show states with predominant d_{yz}, d_{xz} or d_{xy} character in this range (**Figure 2b**, **c** and **S2** in SI), the transitions from the gap states should mainly excite these states. Although the resonant state is not as well localized as the gap state, these states have a substantial overlap, resulting in a high transition probability, which can enhance the photon absorption.[67, 68]

It is interesting to compare the crystal field splittings of Ti 3*d* orbitals in anatase and rutile, see **Figure 3a**. While the overall orbital splittings of *d* orbitals in t_{2g} or e_g are similar in the two polymorphs, the finer splitting of the t_{2g} or e_g manifolds are distinct for the two phases. In particular, the excess electron donated by a *n*-type defect occupies a d_{xy} orbital in rutile[19], while the same kind of excess electron occupies a d_{xz} or d_{yz} orbital in anatase. The octahedral TiO_6 units for anatase and rutile are shown in **Figure 3b, c**. The octahedral field of rutile is almost perfect. The two apical Ti-O bonds along the main axis are about 1.98 Å, while the four equatorial Ti-O bonds form a square with a slightly smaller bond length of 1.949 Å. An excess electron forming a Ti^{3+} ion in rutile occupies a d_{xy} orbital; this affects the four nearby equatorial Ti-O bonds, which become all slightly elongated.[32, 69] The octahedral field of anatase is significantly more distorted in comparison to rutile. The mirror plane symmetry perpendicular to the apical bonds (~1.973 Å) is lost, and the four equatorial Ti-O bonds (~1.93 Å) are not in a plane. For a Ti^{3+} ion with an excess electron in d_{xz} or d_{yz}, only the two equatorial bonds in the plane of the occupied orbital become longer, about 1.962 Å on average, making the distortion of the TiO_6 unit even more pronounced.

We can further compare the characteristics of Ti^{3+} ions in anatase and rutile by considering the projected DOS and oscillator strengths for the pristine and reduced R-TiO_2(110) surfaces. Results obtained using different hybrid functionals are shown in **Figure 4** and **Figure S5** (SI). Similar to anatase, the oscillator strengths of the

VBM→CB transitions on R-TiO_2(110) (**Figure 4 a, d**) are very small in comparison to the transitions from the defect-induced gap states to the CB. The positions of the oscillator strength peaks for the reduced rutile surface correspond to the region of d_{xz} and d_{yz} states in the projected DOS of Ti^{3+} ions, implying that transitions mainly occur from d_{xy} to d_{xz} or d_{yz}. At variance with anatase, the overall distribution of oscillator strengths on reduced R-TiO_2(110) shows a significant dependence on the functional used; for example, HSE06 and $1/\epsilon_\infty$ PBE0 yields a series of peaks of similar intensity between 1 and 2.5 eV (**Figure 4e, f**), while B3LYP results show a prominent sharp feature at ~ 2.5 eV (**Figure S3 d**), which appears to be in better agreement with the resonant feature observed in 2PPE. These differencese can be related to the different localization of the corresponding defect states, which are predicted to be significantly more localized using B3LYP (see **Figure S3** in SI) than HSE06 or $1/\epsilon_\infty$ PBE0.

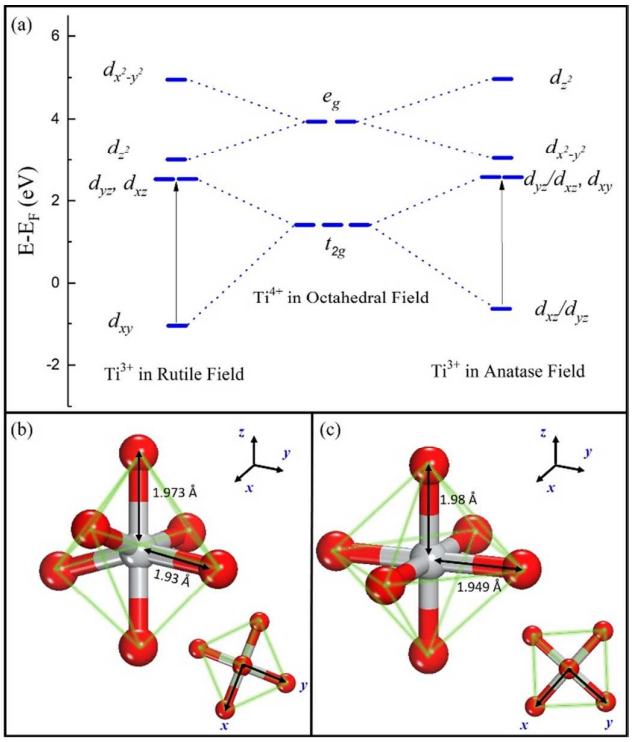

Figure 4 (a) Schematic splitting of the Ti 3*d* orbitals in a perfectly octahedral crystal field (center), rutile (left), and anatase (right). Possible localized *d-d* transitions are also indicated. Energies are referred to the Fermi level E_F. The different energies of the sub-orbitals have been determined from the center of mass energies in the corresponding DOS (**Figure 2b** and **Figure 4b**). (b, c) Primitive octahedral TiO_6 units in anatase and rutile, respectively; top views are shown in the lower right corner. The insets in b, c show the coordinate systems used to distinguish the different *d* sub-orbitals. Red and grey spheres represent titanium and oxygen, respectively.

From the oscillator strengths, the imaginary parts of the dielectric function $\epsilon_2(\omega)$ of reduced anatase and rutile were also determined. As shown in **Figure S4**, the computed absorption edge is at about 1.0 eV for reduced anatase, while it is at somewhat higher energy, ~ 1.5 eV for reduced rutile. This result, combined with the longer electron-hole recombination time at anatase (101) in comparison to rutile (110)[70] (see also the computed surface band structure in **Figure S5**) supports the conclusion that reduced anatase is a better photocatalyst than rutile.

The spatial distributions of gap and excited states on *R*-TiO_2(110) are shown in **Figure S1c** (SI). Independent of the hybrid functional used, the excess electrons are always localized in the subsurface of *R*-TiO_2(110), in agreement with previous studies.[71, 72] Comparison of the defect state energy levels in anatase and rutile (**Table S1**) shows that levels computed with the same theoretical approach are always deeper in rutile than in anatase, in agreement with the experimental finding in **Figure 1e**.

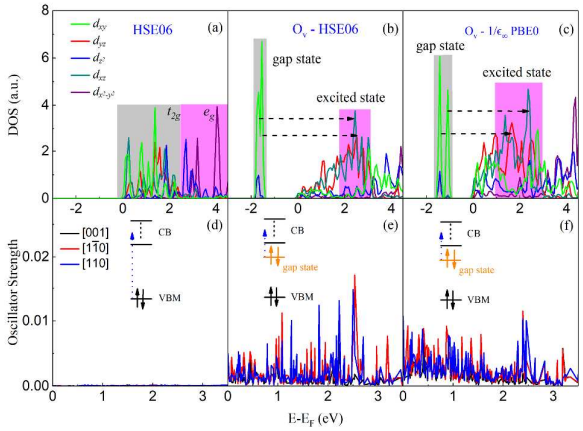

Figure 3 Projected DOS (upper panels) and oscillator strengths (lower panels) of: (a, d) Ti^{4+} ions in pristine rutile TiO_2 (110), from HSE06 calculations; (b, e) and (c, f) Ti^{3+} ions in the rutile (110) slab with one surface O-vacancy, from HSE06 and $1/\epsilon_\infty$ PBE0 (α = 15.8%) calculations, respectively. In (a), the grey and pink regions correspond to the t_{2g} and e_g states, respectively. In (b, c), the grey and pink regions represent the occupied gap state and empty resonant state, respectively. In (d), the oscillator strengths refer to transitions from the VBM state to the CB (blue dashed arrow). In (e, f) the oscillator strengths refer to transitions from the gap states to the CB. The black, red and blue lines indicate the [001], [1$\bar{1}$0] and [110] components, respectively. Simplified MOs or transitions near the band gap are illustrated in each panel.

Polarization dependence of 2PPE signal

Another interesting consequence of the different crystal field splittings in anatase and rutile is the different direction of the transition dipole in the two polymorphs. As shown in **Figure 2** and **4**, the transition dipoles on *R*-TiO_2(110) are mainly along [110] and [1$\bar{1}$0], i.e. perpendicular to the surface and along a surface symmetry direction, while the intensities are strongest mainly along [010] on *A*-TiO_2(101). To verify these predictions, the polarization dependence of the 2PPE excited resonance signal on *A*-TiO_2 was measured (**Figure 5**). In our experimental configuration, the incident plane is the horizontal (XZ) plane along the X axis, which forms a 30-degrees angle with the [010] direction, as revealed by LEED (**Figure 5b**). Based on the electric field of the laser light and the direction, [010], of the calculated transition dipole momentum, the maximum excitation on *A*-TiO_2(101) is expected at Φ = 34.5 degrees (see details in SI). As shown in **Figure 5c**, the secondary electrons signal, proportional to the substrate absorption,[73] displays a maximum and a minimum at 0 (*p*-polarization) and 90 degrees (*s*-polarization), respectively. To exclude the effect of light absorption on the polarization dependent excited resonance, the 2PPE spectra were normalized at the work function edge before the excited

resonance was integrated. The resulting spectra show that though both *p* and *s* polarized light can induce the excitation, the *p*-polarization is more efficient than *s*-polarization on *A*-TiO_2(101).

The polarization dependence of the 2PPE excited resonance signal for the *R*-TiO_2(110) surface has been reported previously.[19] The predicted transition dipole moments for this surface are along [1$\bar{1}$0] and [110]. When the laser light is incident along the [1$\bar{1}$0] (X) or [110] (Z) direction, the maximal intensity is expected at Φ = 0 (see SI). This means that *p* polarized light can yield an excited resonance maximum, which agrees well with experiment.

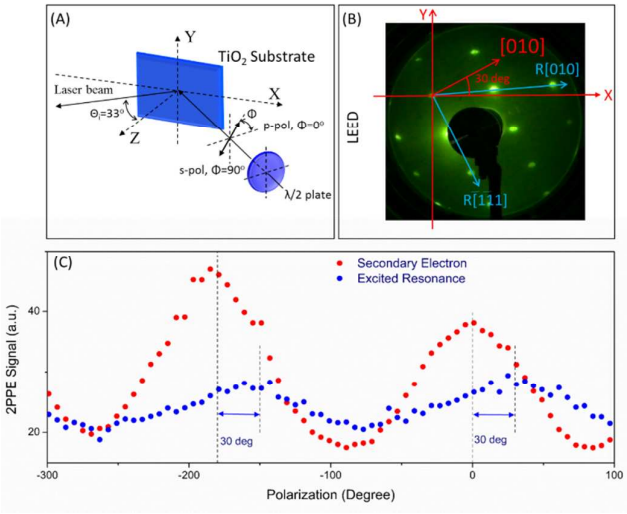

Figure 5 (a) 2PPE experimental configuration showing the incident plane (XZ) and the polarization of the laser light. The incidence angle is 33 degrees. The electric field of *p*-polarized light is along the X axis and the surface normal, while that of *s*-polarized light is along the Y axis. (b) (1 × 1) LEED pattern of the *A*-TiO_2(101) surface. The light blue arrows and words label the directions in the reciprocal space, whereas those in red represent the direction in the real space. The [010] direction deviates from the X axis by about 30 degrees. (c) Dependence of the 2PPE signal on the laser light polarization. Both secondary electron signal (red dots) and the excited resonance (blue dots) are integrated from -5 degrees to +5 degrees. The secondary electron signal is integrated directly at the work function edge. While the excited resonance signal is integrated from the 2PPE spectra which are normalized at the work function edge to correct the absorbance variation induced by polarization tuning. The zero point on the bottom axis stands for the *p*-polarization. The maxima of excited resonance deviates from the *p*-polarization by about 30 degrees due to the specific configuration of the laser plane and the orientation of *A*-TiO_2(101) surface as specified in (b).

Conclusions

Our comparative study of the electronic properties and photoabsorption of the reduced anatase (101) and rutile (110) surfaces has highlighted several similarities as well as significant differences in the characteristics of Ti^{3+} ions in the two materials. Our 2PPE measurements on anatase (101) show a Ti^{3+} induced excited state resonance at about 2.5 eV above E_F that is similar in energy and shape to the one observed on the reduced rutile (110) surface. First principles calculations confirm the presence of Ti^{3+} derived resonant states in a range of about 2.0-3.0 eV above the CBM on both surfaces, and further show that transitions from the gap state to the CB have pronounced peaks of the oscillator strengths in correspondence of the resonant states. Because of the different crystal field splittings in rutile and anatase, the peaks correspond to transitions between d_{xz} and d_{yz} orbitals in anatase, and from d_{xy} to d_{xz} orbitals in rutile, explaining the polarization dependence of 2PPE intensities on the rutile and anatase surfaces. Our results also show that the Ti^{3+} induced occupied states in the band gap are shallower in anatase than in rutile, and $d \rightarrow d$ transitions from the occupied band gap state to the empty Ti^{3+} excited states occur at lower energy in anatase than in rutile (**Figure 6**). Most importantly, our study provides clear evidence that $d \rightarrow d$ transitions in anatase can reduce the threshold of photoabsorption to values well below 3 eV, which can explain the observed photocatalytic activity of Ti^{3+} self-doped anatase under visible light.

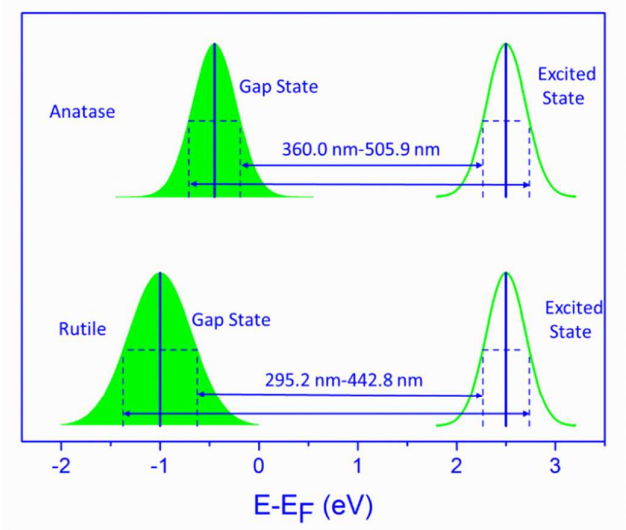

Figure 6 Schematic diagram of the electronic structure of Ti^{3+} ions in anatase and rutile TiO_2. The resonant *d-d* transitions from the band gap states to the Ti^{3+} excited states occur at 3.03 eV and 3.55 eV in anatase and rutile, respectively. The broad distribution of both the gap and excited states extend the photoabsorption to a wide range, covering part of the visible region.

Conflicts of interest

The authors declare no conflicts of interests.

Acknowledgements

This work was supported by the National Natural Science Foundation of China (Grant Nos. 51572016, U1530401, 21573225 21703164 and 21203189), the Ministry of Science and Technology of China (Grant No. 2013CB834605), the National Key Research and Development Program of China (Grant No. 2016YFB0700700 and 2016YFA0200602) and the Youth Innovation Promotion Association of CAS (2017224). A.S. acknowledges the support of DoE-BES, Division of Chemical Sciences, Geosciences and Biosciences under Award DE-SC0007347. We acknowledge computational resources from the Beijing Computational Science Research Center (CSRC).

References

1 A. Fujishima and K. Honda, *Nature*, 1972, **238**, 37-38.
2 U. Diebold, *Surf. Sci. Rep.*, 2003, **48**, 53-229.
3 M. Gratzel, *Nature*, 2001, **414**, 338-344.
4 M. A. Henderson and I. Lyubinetsky, *Chem. Rev.*, 2013, **113**, 4428-4455.
5 M. Ni, M. K. H. Leung, D. Y. C. Leung and K. Sumathy, *Renewable and Sustainable Energy Reviews*, 2007, **11**, 401-425.
6 Q. Guo, C. Zhou, Z. Ma, Z. Ren, H. Fan and X. Yang, *Chem. Soc. Rev.*, 2015, **45**, 3701-3730.
7 W. Zhang, L. Zou, R. Lewis and D. Dionysio, *Journal of Materials Science and Chemical Engineering*, 2014, **02**, 28-40.
8 S. W. Verbruggen, *Journal of Photochemistry and Photobiology C: Photochemistry Reviews*, 2015, **24**, 64-82.
9 K. Maeda and K. Domen, *The Journal of Physical Chemistry Letters*, 2010, **1**, 2655-2661.
10 R. Asahi, T. Morikawa, T. Ohwaki, K. Aoki and Y. Taga, *Science*, 2001, **293**, 269-271.
11 H. H. Pham and L.-W. Wang, *Phys. Chem. Chem. Phys.*, 2015, **17**, 11908-11913.
12 X. Ma, Y. Dai, W. Wei, B. Huang and M.-H. Whangbo, *The Journal of Physical Chemistry Letters*, 2015, **6**, 1876-1882.
13 C. Di Valentin and G. Pacchioni, *Catal. Today*, 2013, **206**, 12-18.
14 C. Di Valentin, G. Pacchioni and A. Selloni, *Phys. Rev. B*, 2004, **70**, 085116.
15 B. Santara, P. K. Giri, K. Imakita and M. Fujii, *J. Phys. Chem. C*, 2013, **117**, 23402-23411.
16 X. Liu, S. Gao, H. Xu, Z. Lou, W. Wang, B. Huang and Y. Dai, *Nanoscale*, 2013, **5**, 1870-1875.
17 F. Zuo, L. Wang, T. Wu, Z. Zhang, D. Borchardt and P. Feng, *J. Am. Chem. Soc.*, 2010, **132**, 11856-11857.
18 L. Liu, P. Y. Yu, X. Chen, S. S. Mao and D. Z. Shen, *Phys. Rev. Lett.*, 2013, **111**, 065505.
19 Z. Wang, B. Wen, Q. Hao, L.-M. Liu, C. Zhou, X. Mao, X. Lang, W.-J. Yin, D. Dai, A. Selloni and X. Yang, *J. Am. Chem. Soc.*, 2015, **137**, 9146-9152.
20 T. Lin, C. Yang, Z. Wang, H. Yin, X. Lü, F. Huang, J. Lin, X. Xie and M. Jiang, *Energy Environ. Sci.*, 2014, **7**, 967.
21 Z. Wang, C. Yang, T. Lin, H. Yin, P. Chen, D. Wan, F. Xu, F. Huang, J. Lin, X. Xie and M. Jiang, *Energy Environ. Sci.*, 2013, **6**, 3007-3014.
22 B. Li, J. Zhao, K. Onda, K. D. Jordan, J. Yang and H. Petek, *Science*, 2006, **311**, 1436-1440.
23 K. Onda, B. Li, J. Zhao, K. D. Jordan, J. Yang and H. Petek, *Science*, 2005, **308**, 1154-1158.
24 Y. Zhang, D. T. Payne, C. L. Pang, H. H. Fielding and G. Thornton, *J. Phys. Chem. Lett.*, 2015, **6**, 3391-3395.
25 A. Argondizzo, S. Tan and H. Petek, *J. Phys. Chem. C*, 2016, **120**, 12959-12966.
26 D. T. Payne, Y. Zhang, C. L. Pang, H. H. Fielding and G. Thornton, *Top. Catal.*, 2016, **60**, 392-400.
27 Y. He, O. Dulub, H. Cheng, A. Selloni and U. Diebold, *Phys. Rev. Lett.*, 2009, **102**, 106105.
28 H. Cheng and A. Selloni, *Phys. Rev. B*, 2009, **79**, 092101.
29 P. Deák, B. Aradi and T. Frauenheim, *Phys. Rev. B*, 2012, **86**, 195206.
30 P. Deák, J. Kullgren and T. Frauenheim, *physica status solidi (RRL) - Rapid Research Letters*, 2014, **8**, 583-586.
31 S. Moser, L. Moreschini, J. Jacimovic, O. S. Barisic, H. Berger, A. Magrez, Y. J. Chang, K. S. Kim, A. Bostwick, E. Rotenberg, L. Forro and M. Grioni, *Phys. Rev. Lett.*, 2013, **110**, 196403.
32 M. Setvin, C. Franchini, X. Hao, M. Schmid, A. Janotti, M. Kaltak, C. G. Van de Walle, G. Kresse and U. Diebold, *Phys. Rev. Lett.*, 2014, **113**, 086402.
33 S. Selcuk and A. Selloni, *Nat. Mater.*, 2016, **15**, 1107-1112.
34 S. Livraghi, M. Chiesa, M. C. Paganini and E. Giamello, *J. Phys. Chem. C*, 2011, **115**, 25413-25421.
35 Z. F. Ren, C. Y. Zhou, Z. B. Ma, C. L. Xiao, X. C. Mao, D. X. Dai, J. LaRue, R. Cooper, A. M. Wodtke and X. M. Yang, *Chinese Journal of Chemical Physics*, 2010, **23**, 255-261.
36 J. VandeVondele, M. Krack, F. Mohamed, M. Parrinello, T. Chassaing and J. Hutter, *Comput. Phys. Commun.*, 2005, **167**, 103-128.
37 S. Goedecker, M. Teter and J. Hutter, *Phys. Rev. B*, 1996, **54**, 1703-1710.
38 J. VandeVondele and J. Hutter, *J Chem Phys*, 2007, **127**, 114105.
39 A. V. Krukau, O. A. Vydrov, A. F. Izmaylov and G. E. Scuseria, *J. Chem. Phys.*, 2006, **125**, 224106.
40 M. Guidon, J. Hutter and J. VandeVondele, *J. Chem. Theory Comput.*, 2009, **5**, 3010-3021.
41 C. Adamo and V. Barone, *J. Chem. Phys.*, 1999, **110**, 6158-6170.
42 S. Kokott, S. V. Levchenko, P. Rinke and M. Scheffler, *New Journal of Physics*, 2018, **20**, 033023.
43 J. P. Perdew, M. Ernzerhof and K. Burke, *J. Chem. Phys.*, 1996, **105**, 9982-9985.
44 M. Gerosa, C. E. Bottani, L. Caramella, G. Onida, C. Di Valentin and G. Pacchioni, *Phys. Rev. B*, 2015, **91**, 155201.
45 J. R. Rumble, *CRC Handbook of Chemistry and Physics*, CRC Press/Taylor & Francis, Boca Raton, FL.
46 R. J. Gonzalez, R. Zallen and H. Berger, *Phys. Rev. B*, 1997, **55**, 7014-7017.
47 K. Kim and K. D. Jordan, *J. Phys. Chem.*, 1994, **98**, 10089-10094.
48 P. J. Stephens, F. J. Devlin, C. F. Chabalowski and M. J. Frisch, *J. Phys. Chem* 1994, **98**, 11623.
49 D. Pan, Q. Wan and G. Galli, *Nature Communications*, 2014, **5**, 3919.
50 K. M. Glassford and J. R. Chelikowsky, *Phys. Rev. B*, 1992, **45**, 3874-3877.
51 P. YU and M. Cardona, *Fundamentals of Semiconductors: Physics and Materials Properties*, Springer Berlin Heidelberg, 2010.
52 Y. B. He, O. Dulub, H. Z. Cheng, A. Selloni and U. Diebold, *Physical Review Letters*, 2009, **102**, 106105.
53 C. Y. Zhou, Z. F. Ren, S. J. Tan, Z. B. Ma, X. C. Mao, D. X. Dai, H. J. Fan, X. M. Yang, J. LaRue, R. Cooper, A. M. Wodtke, Z. Wang, Z. Y. Li, B. Wang, J. L. Yang and J. G. Hou, *Chemical Science*, 2010, **1**, 575-580.
54 Q. Guo, C. Xu, Z. Ren, W. Yang, Z. Ma, D. Dai, H. Fan, T. K. Minton and X. Yang, *J. Am. Chem. Soc.*, 2012, **134**, 13366-13373.
55 Y. Du, N. G. Petrik, N. A. Deskins, Z. Wang, M. A. Henderson, G. A. Kimmel and I. Lyubinetsky, *Phys. Chem. Chem. Phys.*, 2012, **14**, 3066.
56 S. Suzuki, K.-i. Fukui, H. Onishi and Y. Iwasawa, *Physical Review Letters*, 2000, **84**, 2156-2159.
57 D. T. Payne, Y. Zhang, C. L. Pang, H. H. Fielding and G. Thornton, *Surf. Sci.*, 2016, **652**, 189-194.
58 M. M. Islam, M. Calatayud and G. Pacchioni, *J. Phys. Chem. C*, 2011, **115**, 6809-6814.
59 D. O. Scanlon, C. W. Dunnill, J. Buckeridge, S. A. Shevlin, A. J. Logsdail, S. M. Woodley, C. R. A. Catlow, M. J. Powell, R. G. Palgrave, I. P. Parkin, G. W. Watson, T. W. Keal, P. Sherwood, A. Walsh and A. A. Sokol, *Nat. Mater.*, 2013, **12**, 798-801.
60 X. Mao, X. Lang, Z. Wang, Q. Hao, B. Wen, Z. Ren, D. Dai, C. Zhou, L.-M. Liu and X. Yang, *J. Phys. Chem. Lett.*, 2013, **4**, 3839-3844.
61 A. Argondizzo, X. Cui, C. Wang, H. Sun, H. Shang, J. Zhao and H. Petek, *Phys. Rev. B*, 2015, **91**, 155429.
62 P. Reckers, M. Dimamay, J. Klett, S. Trost, K. Zilberberg, T.

Riedl, B. A. Parkinson, J. Brötz, W. Jaegermann and T. Mayer, *J. Phys. Chem. C*, 2015, **119**, 9890-9898.
63 K. M. Glassford and J. R. Chelikowsky, *Phys. Rev. B*, 1992, **46**, 1284-1298.
64 Z.-T. Wang, J. C. Garcia, N. A. Deskins and I. Lyubinetsky, *Phys. Rev. B*, 2015, **92**, 081402.
65 N. Martsinovich, D. R. Jones and A. Troisi, *J. Phys. Chem. C*, 2010, **114**, 22659-22670.
66 T. R. Esch and T. Bredow, *Surf. Sci.*, 2017, **665**, 20-27.
67 A. T. B. Gilbert, N. A. Besley and P. M. W. Gill, *J. Phys. Chem. A*, 2008, **112**, 13164-13171.
68 N. J. Turro, V. Ramamurthy and J. C. Scaiano, *Modern Molecular Photochemistry of Organic Molecules*, University Science Books, 2010.
69 C. Di Valentin, G. Pacchioni and A. Selloni, *Phys. Rev. Lett.*, 2006, **97**, 166803.
70 A. Nijamudheen and A. V. Akimov, *J. Phys. Chem. C*, 2017, **121**, 6520-6532.
71 N. A. Deskins, R. Rousseau and M. Dupuis, *J. Phys. Chem. C*, 2011, **115**, 7562-7572.
72 P. Krüger, J. Jupille, S. Bourgeois, B. Domenichini, A. Verdini, L. Floreano and A. Morgante, *Phys. Rev. Lett.*, 2012, **108**.
73 M. Wolf, A. Hotzel, E. Knoesel and D. Velic, *Physical Review B*, 1999, **59**, 5926-5935.